ACS APPLIED MATERIALS & INTERFACES

RESEARCH ARTICLE

www.acsami.org

# New Approach to Bone Tissue Engineering: Simultaneous Application of Hydroxyapatite and Bioactive Glass Coated on a Poly(L-lactic acid) Scaffold

Peyman Dinarvand,[†,‡] Ehsan Seyedjafari,[*,§] Abbas Shafiee,[†,‡] Ali Babaei Jandaghi,[⊥] Ali Doostmohammadi,[¶] Mohammad Hossein Fathi,[#] Shirin Farhadian,[▽] and Masoud Soleimani[*,||]

[†]Stem Cell Biology Department, Stem Cell Technology Research Center, Tehran, Iran

[‡]Faculty of Medicine, Tehran University of Medical Sciences, Tehran, Iran

[§]Department of Biotechnology, College of Science, University of Tehran, Tehran, Iran

[⊥]Department of Radiology, Poursina Hospital, Guilan University of Medical Sciences, Rasht, Iran

[¶]Biomaterials Group, Faculty of Engineering, Shahrekord University, Shahrekord, Iran

[#]Biomaterials Research Center, Department of Materials Engineering, Isfahan University of Technology, Isfahan, Iran

[▽]Faculty of Dentistry, Semmelweis University, Budapest, Hungary

[||]Department of Hematology, Faculty of Medical Science, Tarbiat Modares University, Tehran, Iran

**ABSTRACT:** A combination of bioceramics and polymeric nanofibers holds promising potential for bone tissue engineering applications. In the present study, hydroxyapatite (HA), bioactive glass (BG), and tricalcium phosphate (TCP) particles were coated on the surface of electrospun poly(L-lactic acid) (PLLA) nanofibers, and the capacity of the PLLA, BG−PLLA, HA−PLLA, HA−BG−PLLA, and TCP−PLLA scaffolds for bone regeneration was investigated in rat critical-size defects using digital mammography, multislice spiral-computed tomography (MSCT) imaging, and histological analysis. Electrospun scaffolds exhibited a nanofibrous structure with a homogeneous distribution of bioceramics along the surface of PLLA nanofibers. A total of 8 weeks after implantation, no sign of complication or inflammation was observed at the site of the calvarial bone defect. On the basis of imaging analysis, a higher level of bone reconstruction was observed in the animals receiving HA-, BG-, and TCP-coated scaffolds compared to an untreated control group. In addition, simultaneous coating of HA and BG induced the highest regeneration among all groups. Histological staining confirmed these findings and also showed an efficient osseointegration in HA−BG-coated nanofibers. On the whole, it was demonstrated that nanofibrous structures could serve as an appropriate support to guide the healing process, and coating their surface with bioceramics enhanced bone reconstruction. These bioceramic-coated scaffolds can be used as new bone-graft substitutes capable of efficiently inducing osteoconduction and osseointegration in orthopedic fractures and defects.

**KEYWORDS:** electrospinning, bone, bioceramics, hydroxyapatite, bioglass, tricalcium phosphate, calvarial defect

## INTRODUCTION

Bioceramics have been used as classic bone graft substitutes over the last 40 years.[1] The high level of synthetic graft applications comes from the major drawbacks of the two other options for the treatment of bone defects caused by injuries, trauma, or diseases. Autogenic bone graft acts as the gold standard for bone void filling. However, it lacks a sufficient quantity, and the patient will suffer from a second surgery to harvest bone tissue. The transmission of infectious diseases and risk of immunological rejection are the major complications in using allogenic grafts for bone treatments.[2,3] Bioactive glasses (BG) and calcium phosphate based ceramics are the main widely used classes of bioceramics in the field of bone tissue engineering. BG are based on a silicate- or phosphate-forming network with $Na_2O$ and CaO as network modifiers. Their bioactivity enables the use of these types of materials for bone bonding and efficient osteointegration.[4,5] Among the calcium phosphate based materials, hydroxyapatite is the most popular graft substitute widely used to treat bone injuries and damage. Its general formula, $Ca_{10}(OH)_2(PO_4)_6$, is highly similar to the chemical composition of the bone inorganic phase. This resemblance can lead to the strong affinity of hydroxyapatite (HA) to the host bone and high chemical bonding. HA may be prepared from natural bone or coral or be chemically synthesized in various physical forms such as particles, rods, or porous dense blocks.[6] The major drawback of these bioceramics is their inherent brittleness and low mechanical properties, which hinder their use in load-bearing applications. It is also difficult to maintain and shape these materials in the defect site.[7] To address this issue, several works have been performed to combine the bioactivity of bioceramics with the appropriate mechanical properties of other biomaterials such as polymers and metals.[8−11] Among different approaches, the coating of ceramics on the surface of bone implants is a common method to improve their biological characteristics such as bioactivity, osteointegrity, and osteoconductivity.[12,13] In a recent

**Received:** September 7, 2011
**Accepted:** October 17, 2011
**Published:** October 17, 2011

study, we coated the HA nanoparticles on the surface of poly-(L-lactide) (PLLA) nanofibers and showed that this scaffold could enhance osteogenic differentiation of stem cells and induce ectopic bone formation.[14] The ECM-mimicking nanofibrillar nature of electrospun scaffolds is appropriate to support tissue regeneration and integration.[15] We hypothesized that bioceramic-coated electrospun scaffolds can serve as bone graft substitutes for the treatment of bone injuries and defects. Therefore, in the present study, we used bone-derived HA and BG nanopowder to coat the surface of PLLA nanofibrous scaffolds to treat a critical-size calvarial defect in a rat model during the course of an 8 week study period.

## MATERIALS AND METHODS

**Preparation of Bioceramics.** Bioactive glass (BG) and bone-derived hydroxyapatite (HA) were prepared as previously reported from our laboratory.[16] Briefly, for the preparation of BG, colloidal solutions (sols) of 63S composition (63 mol % $SiO_2$, 28 mol % CaO, and 9 mol % $P_2O_5$) were prepared by mixing distilled water, 2 N hydrochloric acid (HCl), tetraethyl orthosilicate (TEOS), triethyl phosphate (TEP), and calcium nitrate. The silica sol was prepared in alcoholic media without a catalyst. The initial procedure involved the mixing of TEOS (28 mL) and ethanol (40 mL) as an alcoholic media. Distilled water was added to solution, and the solution was allowed to mix until it became clear. The $H_2O$/TEOS molar ratio was 4:1. After 30 min, TEP (2.3 mL) was added to the stirring solution. After another 20 min, calcium nitrate (12 g) was added. The solution was then stirred for an additional 1 h. The gel was heated (60 °C, 10 h), dried (130 °C, 15 h), and thermally stabilized (600 °C, 10 h) according to established procedures. The produced gel was milled in order to disagglomerate the particles. For the preparation of HA, an adult bovine femur was obtained from a slaughterhouse and boiled in water for 12 h to render it aseptic and loosen any attached soft tissues. Then, it was washed and cleaned carefully to remove visible tissues, fats, and any other readily visible foreign materials on the bone surface. To remove the internal organic content (e.g., collagen) and water, the bone was then heated in an electric furnace under ambient conditions at 900 °C with a 2 h holding time. The resulting white solid specimens were ground and sieved to reach a particle size of less than 50 $\mu$m.

**Scaffold Preparation.** The nanofibrous scaffolds were prepared via electrospinning as previously reported from our laboratory.[17] PLLA (Sigma Aldrich, St. Louis, MO) was dissolved in chloroform (Merck, Germany) with a 4% (w/v) concentration. A 5 mL syringe was filled with a PLLA solution. The solution was fed into a 20-gauge needle through an extension tube by a syringe pump. The needle was located at a distance of 15 cm from a grounded collector, and a 15-kV voltage was applied to this setup using a high-voltage direct-current power supply (Stem Cell Technology Research Center, Tehran, Iran). Having reached a thickness of about 200 $\mu$m, the mat was detached from the collector and placed in a vacuum for evaporation of the residual solvent. Oxygen plasma treatment was then performed by a low-frequency plasma generator of 44 GHz frequency with a cylindrical quartz reactor (Diener Electronics, Ebhausen, Germany). Pure oxygen was introduced into the reaction chamber at 0.4 mbar pressure, and the glow discharge was ignited for 5 min. A 1% (w/v) solution of HA, BG, and a commercial tricalcium phosphate (TCP) in deionized water was prepared after thorough dispersion in an ultrasonic bath for 20 min. To deposit these materials on the surface of nanofibers, plasma-treated mats were immersed individually in each aqueous solution overnight. After that, the mats were rinsed well with deionized water and dried in a vacuum. All experiments were performed on the following groups: Untreated control group, pristine PLLA nanofibers (PLLA), BG-coated PLLA nanofibers (BG−PLLA), HA-coated PLLA nanofibers (HA−PLLA), BG- and HA-coated PLLA nanofibers (BG−HA−PLLA), and TCP-coated PLLA nanofibers (TCP−PLLA).

**X-ray Diffraction (XRD).** An XRD technique (Philips X'Pert-MPD system with a Cu K$\alpha$ wavelength of 1.5418 Å) was used to analyze the structures of the prepared BG, HA, and TCP. The diffractometer was operated at 40 kV and 30 mA at a 2$\theta$ range of 20−70°, employing a step size of 0.02°/s.

**Scanning Electron Microscopy (SEM).** The surface morphology of scaffolds was characterized using a scanning electron microscope (LEO 1455VP, Cambridge, U.K.) after coating the specimens with gold using a sputter coater. The fiber diameter was determined from SEM images in which the diameter of 100 fibers was measured using image analysis software (image J, NIH, USA).

**Animal Study and Surgical Procedure.** All animal experiments were performed in accordance with the Stem Cell Technology Research Center (Tehran, Iran) guidelines. A total of 60 male Sprague−Dawley rats (10 animals per group, Razi Institute, Karaj, Iran) weighing 200−250 g were housed under standard conditions at a controlled temperature (20 °C) and a light/dark cycle (12/12 h). Rats were individually anesthetized via intraperitoneal injections of ketamine (20 mg/kg) and xylazine (2 mg/kg) and inhaled a mixture of 20% v/v isoflurane and propylene glycol. The implantation of scaffolds was performed in critical-size calvarial defects in a rat model. The surgical site was first shaved and scrubbed with iodine. An incision was then made in the sagittal plane across the cranium. A full-thickness flap including the periosteum was reflected, exposing the calvarial bone. Then, a critical-size (8-mm-diameter) circular and transosseous defect was created on the cranium using a saline-cooled trephine drill. Each defect was filled with a circular scaffold from each group. As a control, the defect was left empty. The incisions were finally closed using absorbable sutures.

**Digital Mammography and Multislice Spiral Computed Tomography (MSCT) Imaging Analysis.** Following an in vivo end time point, the animals were euthanized, and their craniums were excised and placed in 10% formalin. The samples were then radiographed under direct digital mammography equipment (Konica Minolta, Regius model 110HQ). The specimens were also scanned using a spiral high-resolution computed tomography (CT) system (Siemens, SOMATOM Sensation) in multislice mode. The radiograph images from digital mammography were scored by two independent radiologists. To quantify the level of bone regeneration via MSCT, a 9-mm circular region of interest was placed in each CT image. The area of newly formed bone was quantified relative to the original calvarial defect.

**Histological Analysis.** For histological examinations, the fixed samples were decalcified in ethylenediaminetetraacetic acid/HCl and embedded in paraffin. Sections with 3−5-$\mu$m thickness were made and stained with hematoxylin and eosin (HE). The area of newly formed bone was examined under light microscopy and quantified using a computer-assisted Image-Pro Plus System (Media Cybernetics, Silver Springs, MD).

**Statistical Analysis.** All data were reported as mean ± standard deviation (SD). The statistical significance was determined by a Mann−Whitney U test as a nonparametric equivalent of an independent sample Student's $t$ test. Simple one-way analysis of variance and its nonparametric equivalent (Kruskal−Wallis test) were used to compare the results among multiple groups. All analyses were performed using SPSS 17.0 software. A $P$ value of <0.05 was considered to be statistically significant.

## RESULTS

**Characterization of Bioceramics and Scaffolds.** The XRD patterns of prepared BG, HA, and TCP particles are depicted in Figure 1. The XRD pattern of the prepared glass after heating at 600 °C for 10 h did not contain diffraction maxima, indicative of the internal disorder and the glassy nature of this material.

The XRD spectrum also showed that the HA particles prepared from bovine bone and the commercial TCP were highly crystalline.

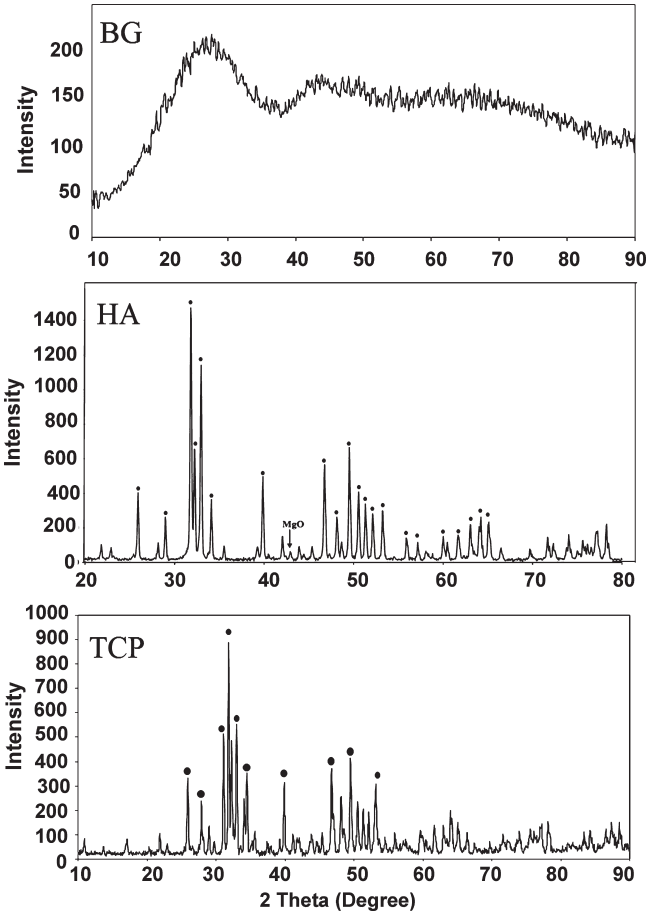


**Figure 1.** XRD pattern of the prepared BG nanoparticles, bone-derived HA, and commercial TCP: intensity of diffraction vs angle of radiation ($2\theta$).

The morphology of electrospun scaffolds and bioceramics was investigated under SEM (Figure 2). The nanofibers showed a randomly oriented uniform morphology with an average diameter of 822 ± 97 nm. After coating, a homogeneous distribution of nanoscale HA and BG along the surface of the nanofibers was observed in all groups. The TCP also had a microsized structure after coating on the surface of PLLA nanofibrous scaffolds.

**In Vivo Bone Regeneration.** *Gross Examinations.* No general or local complications were observed in any of the animals during the study, and all of them survived. No sign of wound fester, infection, scalp edema, or effusion was detected at the site of surgery. A total of 8 weeks after implantation, the specimens were retrieved and used for bone regeneration evaluation. Gross examination of the defects after 8 weeks revealed no sign of inflammation or scaffold disintegration (Figure 3). In an untreated control group, no spontaneous mineralization and bone healing was observed in the defect after the period of study (Figure 3B). All implanted scaffolds were well integrated into the surrounding calvarial bone with no sign of encapsulation or prominent foreign body reaction (Figure 3C). In addition, the scaffolds adhered strongly to the host osseous tissue without any fixation.

*Evaluation of Bone Regeneration.* To evaluate the quantity of newly formed bone, Digital Mammography and MSCT were performed on the fixed calvarium samples retrieved 8 weeks after implantation. The radiographic images of different groups are depicted in Figure 4. Qualitatively, the images show regeneration of defects after implantation of bioceramic-coated nanofibrous scaffolds. The quantitative analysis of the regenerated areas demonstrated that uncoated PLLA nanofibers had no significant healing effect in the bone defects compared to an untreated control. However, a higher amount of new mineralized tissue was measured in groups that received HA−PLLA and BG−PLLA compared to PLLA and untreated control groups ($P < 0.05$), and the TCP−PLLA group enhanced bone formation compared to HA- or BG-coated nanofibers and an untreated control group ($P < 0.05$). The highest regenerated bone was observed for HA−BG−PLLA, which was even higher than that in the rats

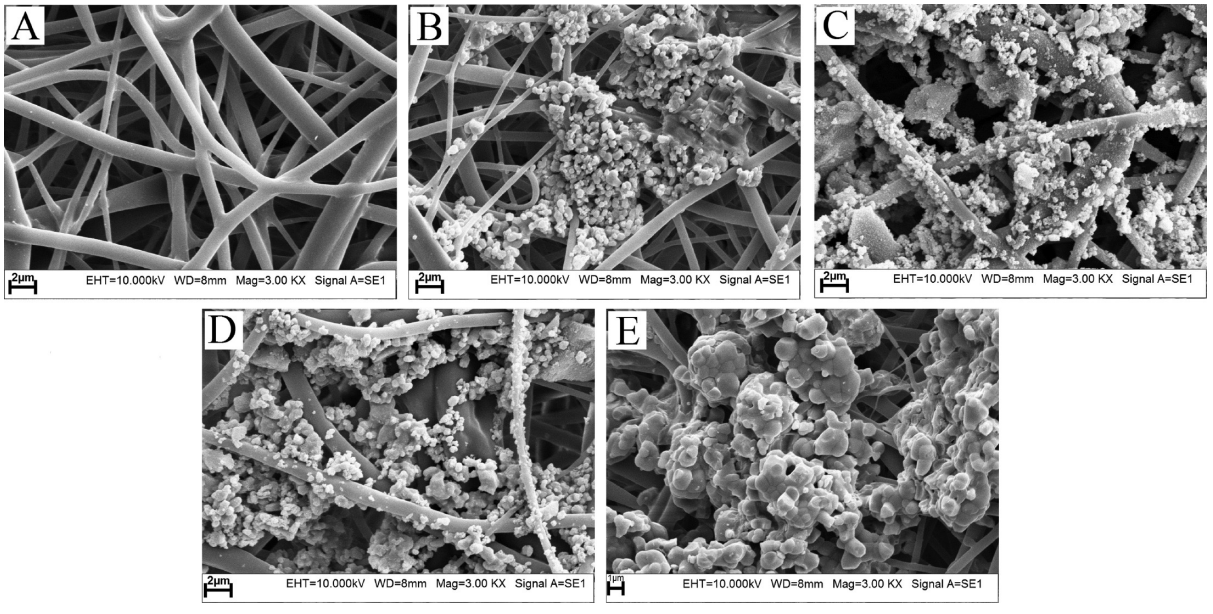


**Figure 2.** Morphology of fabricated scaffolds: PLLA (A), HA−PLLA (B), BG−PLLA (C), HA−BG−PLLA (D), and TCP−PLLA (E).

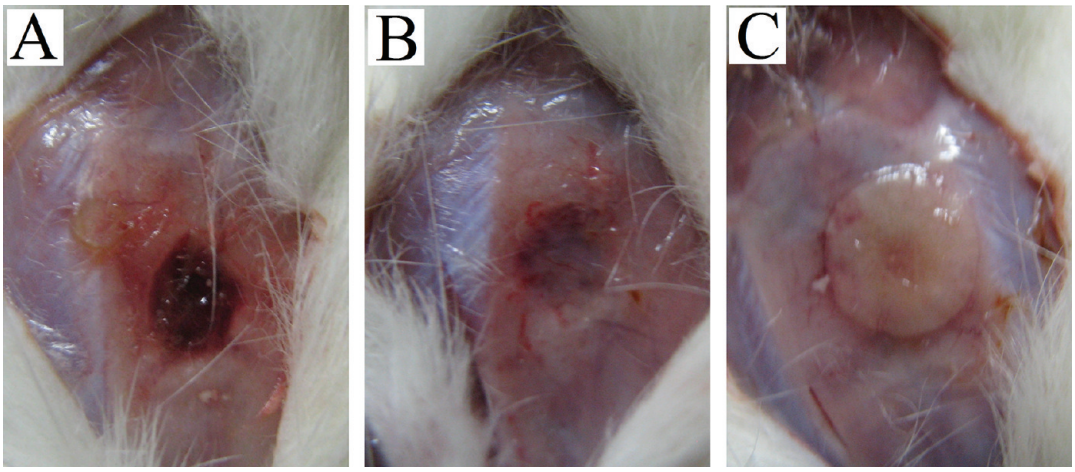


**Figure 3.** Critical-size defect created in rat calvaria (A) and after 8 weeks of study without (B) or with (C) an implanted scaffold.

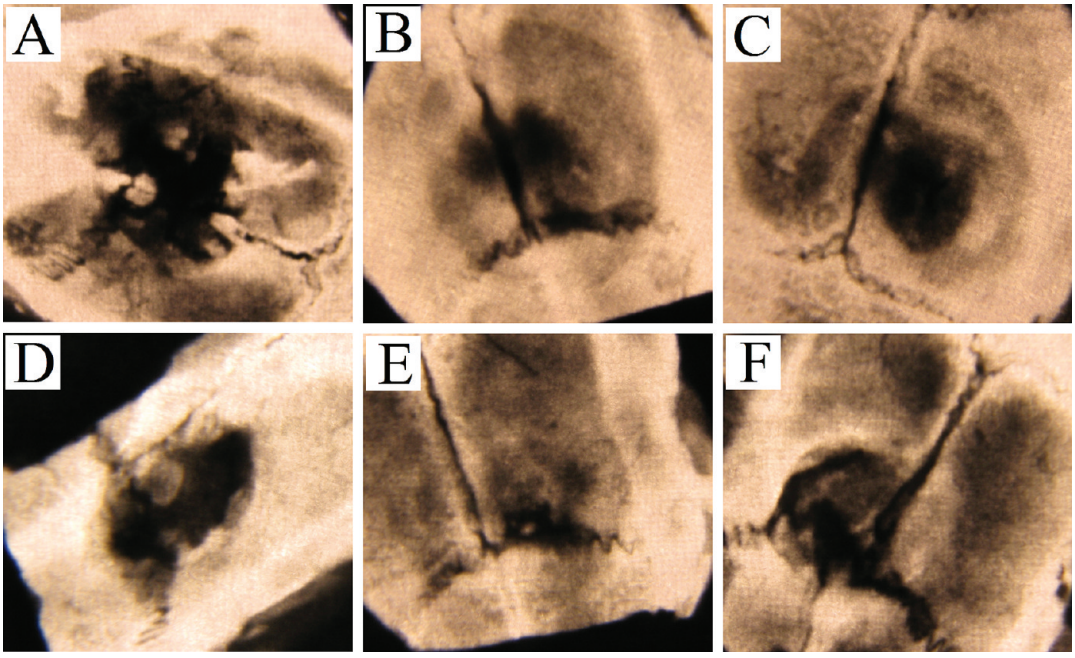


**Figure 4.** Digital mammography images of the rat calvarial after 8 weeks of study: untreated control group (A), PLLA (B), HA−PLLA (C), BG−PLLA (D), HA−BG−PLLA (E), and TCP−PLLA (F).

treated by nanofibers coated with the commercial graft TCP (TCP−PLLA; $P < 0.05$). The area of newly formed bone was also investigated using MSCT (Figure 5). A near-complete regeneration of the calvarial defect was observed in the defects treated with HA−BG−PLLA. However, different levels of void defects were detected in rats that received other nanofibrous scaffolds. The amount of newly formed bone quantified by the imaging software was similar to the results obtained from radiography (data not shown). In both CT and Digital Mammography, regeneration was shown to start from the edges of the defect toward the center. There was also no significant bone formation in untreated control rats, so that the 8-mm-diameter defect was demonstrated to be a critical-size rat calvarial defect in this study.

Finally, a histological evaluation was performed to compare the reconstruction of the damaged bone in experimental animals after 8 weeks of implantation (Figure 6). The area of newly formed bone was shown as mean ± SD and is depicted in Figure 7. The highest amount of newly formed bone was observed in the rats receiving HA−BG−PLLA ($P < 0.05$). In the defects treated with HA−PLLA and BG−PLLA, a similar amount of regenerated tissue was observed, and it was significantly higher than that detected in the control animals ($P < 0.05$).

## DISCUSSION

Osteoconductivity, bioactivity, and suitable mechanical properties are the major requirements for bone graft substitutes.[18] Bioceramics have been shown to be biocompatible and enhance the process of reconstruction in critical-size bone defects.[19−21] However, their poor mechanical characteristics such as intrinsic brittleness hinder their wide-range application for bone regeneration.[7] In our previous study, we successfully coated HA nanoparticles

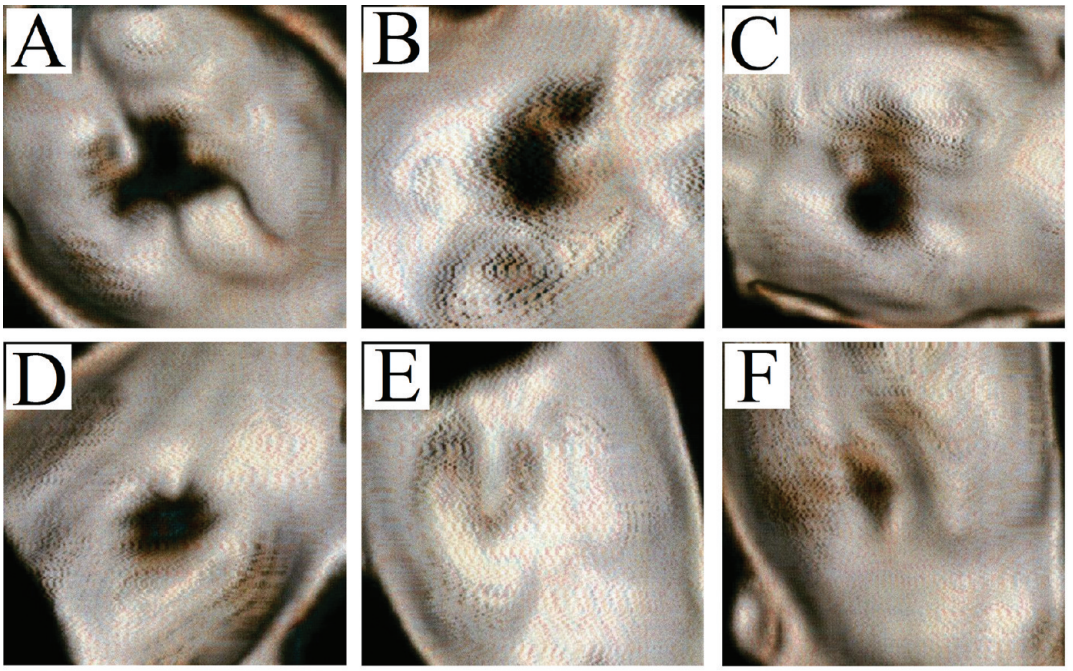


**Figure 5.** MSCT images of the rat calvarial after 8 weeks of study: untreated control group (A), PLLA (B), HA−PLLA (C), BG−PLLA (D), HA−BG−PLLA (E), and TCP−PLLA (F).

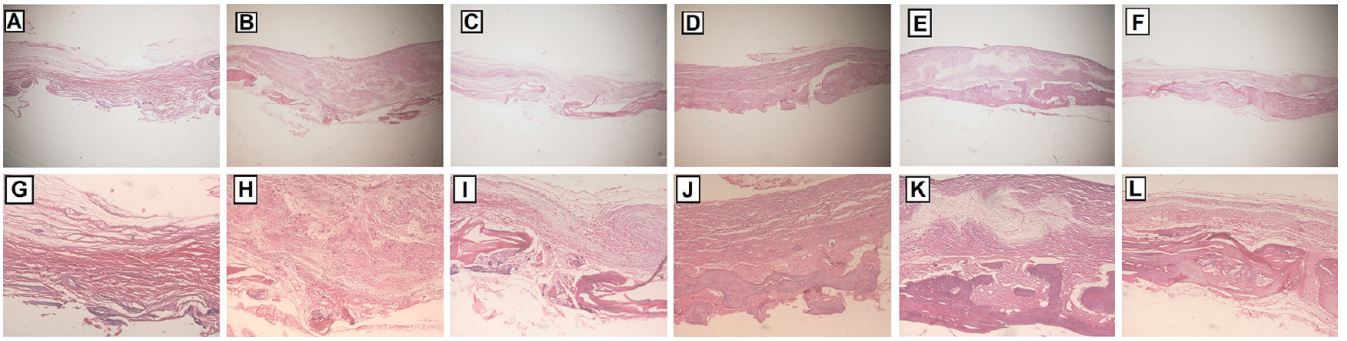


**Figure 6.** Optical micrographs of the defects stained with HE: untreated control group (A and G), PLLA (B and H), HA−PLLA (C and I), BG−PLLA (D and J), HA−BG−PLLA (E and K), and TCP−PLLA (F and L) with two magnifications, (A−F) 10× and (G−L) 40×.

on the surface of electrospun PLLA nanofibers.[14] Then we showed that the osteogenic differentiation of stem cells was enhanced when cultured on this structure compared to uncoated scaffolds and TCP. Interestingly, we demonstrated that nano-HA-coated scaffolds could induce ectopic bone formation after 8 weeks of subcutaneous implantation in mice.[14] In the present study, we aimed to investigate the osteocondctivity of bioceramic-coated nanofibrous scaffolds implanted in rat calvarial defects. Herein, we used two types of bioceramics fabricated in our laboratory, BG and HA. The process of fabrication, physiochemical properties, and in vitro cytocompatibility of these bioceramics has been reported in our previous studies.[16,22,23] Coating of implants with osteoconductive and osteoinductive materials is one of the major strategies to improve their bioactivity and biological properties.[24,25] Along this line, several studies have reported the highly efficient in vitro and in vivo performances of bone implants coated with bioceramics such as HA and BG. Bigi et al. demonstrated the improved attachment of bone to the surface of an HA-coated alloy implant.[26] In another study, enhancement of the osseointegration of a poly(ethylene terephthalate) graft coated with 58S BG was observed in a bone tunnel.[27] There are several reports in which the researchers have used electrospun nanofibrous scaffolds with different modifications for bone tissue engineering applications.[28] In a few of them, the surface of fibers has been coated with calcium phosphate cements or HA to improve the bioactivity of the electrospun scaffold. However, none of them has investigated the osteoconductivity of these structures in an animal model. For instance, Mavis et al. immersed the PCL nanofibers in calcium phosphate solutions similar to simulated body fluids and observed deposition of a biomimetic calcium phosphate layer on the nanofibers.[29] In another study, PLLA nanofibrous mats were soaked in a similar solution, and the in vitro culture and differentiation of preosteoblasts were investigated.[30] The deposition of calcium phosphate ceramics has also been accomplished on recombinant spider silk electrospun fibers by Yang et al.[31] The in vivo

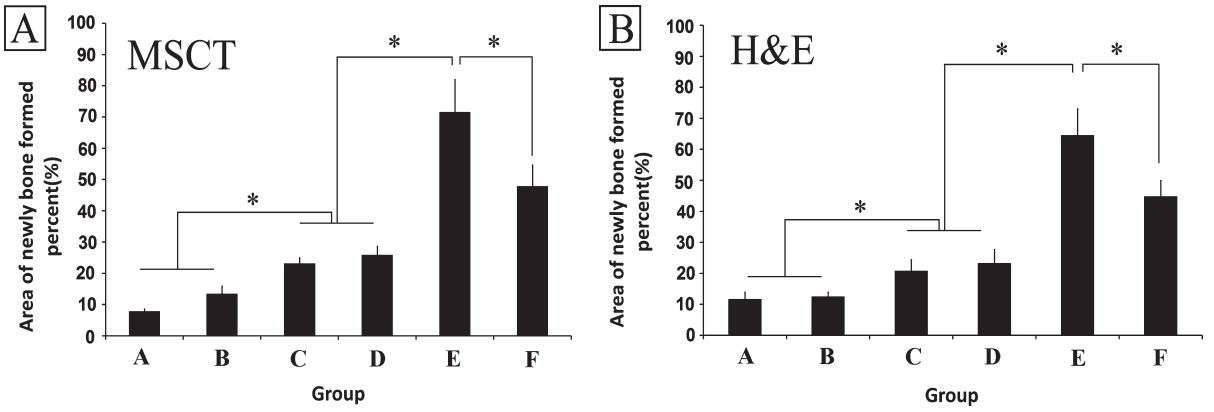


**Figure 7.** Area of newly formed bone resulting from the quantification of MSCT (A) and HE (B) data. The significant difference ($P < 0.05$) has been shown between the groups indicated by asterisks. Groups specified are an untreated control group (A), PLLA (B), HA−PLLA (C), BG−PLLA (D), HA−BG−PLLA (E), and TCP−PLLA (F).

performance of electrospun nanofibers coated with HA-like materials was also studied in a report by the same research group.[32] There, the osteoinduction of calcium phosphate coated electrospun scaffolds seeded with mesenchymal stem cells was demonstrated after subcutaneous implantation in goats. Not only is our study the first report on the coating of the surface of electrospun nanofibers with BG nanoparticles, but also the HA extracted from animal bone was applied for in vivo experiments. In some recent reports, BG particles were inserted inside the polymeric fibers via the electrospinning of the polymer/BG solutions. These composite scaffolds have shown increased biocompatibility and osteoconductivity in comparison to the pristine nanofibers.[33] In a recent study, Noh et al. fabricated PLLA electrospun nanofibers containing nanosized BG and showed the improved adhesion and culture of osteoblasts on the surface of nanofibrous scaffolds.[34] BG has been also processed via electrospinning to form ultrafine nanofibers for bone regeneration applications.[35,36]

The XRD pattern of the fabricated BG showed the amorphous nature of the nanoparticles, characterized by the broad diffraction bands. Our finding also demonstrated that there was no crystalline phase in BG particles in complete agreement with previous reports.[37,38] In contrast to BG nanoparticles, HA and TCP particles exhibited a highly crystalline ceramic structure explained by their XRD patterns. The HA spectra ($2\theta = 31.83°$) exactly conform to the bone-derived HA XRD pattern that is reported in the literature.[39] Also, only a minimal amount of MgO ($2\theta = 42.9°$) was detected in the XRD pattern. This result is in agreement with previous reports.[40] There was no CaO detectable by XRD. The fabricated nanofibrous scaffolds showed a highly porous appearance with interconnected pores. This type of structure is very appropriate for an efficient bone bonding and osteointegration resulting from the infiltration and growth of the surrounding host tissue through the inside of the implant.[41] Bone is a complex organization of collagen nanofibrils incorporated with natural ceramics similar in composition to HA.[42] The bioceramic-coated PLLA nanofibers prepared in this study can efficiently mimic the natural ECM in the bone tissue. The SEM data also confirmed the coating of bioceramics on the surface of PLLA nanofibers. After repeated rinsing, the ceramic particles remained attached except the loosely adhered particles released to the washing medium during rinsing. After surface plasma treatment, the scaffolds became highly hydrophilic because of the formation of surface anionic chemical groups. The electrostatic bonds between them and the cationic groups existing in bioceramics can be the reason for the attachment of HA and BG to the surface of plasma-treated nanofibers.[43] From a gross view, no sign of inflammation was observed in the site of implantation for any of the scaffolds. This observation was confirmed by a histological study and showed the in vivo biocompatibility of our scaffolds in the rat model. Two independent quantitative methods were used to measure the amount of mineralization and bone regeneration during implantation. Interestingly, similar results were found from both Digital Mammography and MSCT, which demonstrated that the HA−BG−PLLA scaffold induced the highest level of reconstruction compared to that resulting from other scaffolds. A similar amount of mineralization was detected in critical-size defects implanted with HA−PLLA and BG−PLLA. BG and HA have been extensively reported as osteoconductive materials that induce regeneration of bone defects.[44] In this study, we showed that polymeric nanofibers coated with these materials could also serve as osteoconductive scaffolds. Lin et al. compared the capacity of porous HA and BG as bone substitutes in femoral condyle of rabbits and demonstrated the higher level of regeneration after 8 weeks of bioglass implantation.[45] Wheeler et al. also found higher bone ingrowths in rabbit femur treated with 45S5 glass-coated implants compared to those coated with HA after 12 weeks of implantation.[46] According to our study, these authors did not observe any significant differences between BG- and HA-coated implants compared to a control (empty defect) until this time point. In a recent clinical study, Mistry et al. showed that BG-coated implants were as equally successful as HA-coated implants in achieving osseointegration to support final restorations in the human jaw bone.[47] Interestingly, the HA−BG−PLLA scaffold induced a significantly higher level of reconstruction compared to that observed in defects treated with TCP−PLLA. TCP is an osteoconductive grafting material that has generally been used as a bone filler in orthopedic applications.[48] In addition, we demonstrated that our fabricated HA−BG−PLLA scaffolds synergistically enhanced bone regeneration higher than that observed for BG−PLLA and HA−PLLA. There are some studies that have attempted to enhance the bioactivity and bone-bonding strength of implants coated simultaneously with BG and HA. Yamada et al. demonstrated both the biocompatibility and osteoconductivity of titanium implants coated with HA and

BG prepared by the cullet method.[49] Lin et al. have also investigated the bioactivity improvement effect of a HA−BG composite coating formed by plasma spraying on a commercial implant.[50] Finally, our results from Digital Mammography and MSCT were confirmed by pathological evaluations. In addition, penetration of the newly formed bone into the nanofibrous scaffolds obviously indicated the capability of HA−BG−PLLA scaffolds to induce an efficient amount of osteointegration, which is critical for an appropriate healing of orthopedic fractures and defects.

## CONCLUSION

In this study, we demonstrated that nanofibrous structures could be used as an appropriate support to guide bone regeneration. In addition, nanofibers simultaneously coated with HA and BG hold promising potential as efficient osteoconductive implants for bone tissue engineering applications.

## AUTHOR INFORMATION

### Corresponding Author

*Tel: +98-21-66491622 (E.S.), +98(21)88861065-7 (M.S.). Fax: +98-21-66491622 (E.S.), +98-21-8886-1065-7 (M.S.). E-mail: seyedjafari@ut.ac.ir (E.S.), soleim_m@modares.ac.ir (M.S.).

## ACKNOWLEDGMENT

The authors would like to acknowledge the financial support of University of Tehran for this research.

## REFERENCES

(1) Laurencin, C. *Bone graft substitutes*; ASTM International: West Conshohocken, PA, 2003; p 260.
(2) Betz, R. R. *Orthopedics* **2002**, *25*, 561–570.
(3) Giannoudis, P. V.; Dinopoulos, H.; Tsiridis, E. *Injury* **2005**, *36*, 20–27.
(4) Hench, L. L. *J. Mater. Sci.: Mater. Med.* **2006**, *17*, 967–978.
(5) Hench, L. L.; Polak, J. *Mater. Sci.* **2002**, *295*, 1014–1017.
(6) LeGeros, R. Z. *Chem. Rev.* **2008**, *108*, 4742–4753.
(7) Best, S.; Porter, A.; Thian, E.; Huang, J. *J. Eur. Ceram. Soc.* **2008**, *28*, 1319–1327.
(8) Francis, L.; Meng, D.; Knowles, J. C.; Roy, I.; Boccaccini, A. R. *Acta Biomater.* **2010**, *6*, 2773–2786.
(9) Gaharwar, A. K.; Dammu, S. A.; Canter, J. M.; Wu, C. J.; Schmidt, G. *Biomacromolecules* **2011**, *12*, 1641–1650.
(10) Pamula, E.; Kokoszka, J.; Cholewa-Kowalska, K.; Laczka, M.; Kantor, L.; Niedzwiedzki, L.; Reilly, G. C.; Filipowska, J.; Madej, W.; Kolodziejczyk, M.; Tylko, G.; Osyczka, A. M. *Ann. Biomed. Eng.* **2011**, *39*, 2114–2129.
(11) Wang, X.; Song, G.; Lou, T. *J. Mater. Sci.: Mater. Med.* **2010**, *21*, 183–188.
(12) Ballarre, J.; Manjubala, I.; Schreiner, W. H.; Orellano, J. C.; Fratzl, P.; Cere, S. *Acta Biomater.* **2010**, *6*, 1601–1609.
(13) Facca, S.; Lahiri, D.; Fioretti, F.; Messadeq, N.; Mainard, D.; Benkirane-Jessel, N.; Agarwal, A. *ACS Nano* **2011**, *5*, 4790–4799.
(14) Seyedjafari, E.; Soleimani, M.; Ghaemi, N.; Shabani, I. *Biomacromolecules* **2010**, *11*, 3118–3125.
(15) Smith, L.; Ma, P. *Colloids Surf., B* **2004**, *39*, 125–131.
(16) Doostmohammadi, A.; Monshi, A.; Fathi, M. H.; Golniya, Z.; Daniels, A. *Ceram. Int.* **2011**, *37*, 2311–2316.
(17) Seyedjafari, E.; Soleimani, M.; Ghaemi, N.; Sarbolouki, M. N. *J. Mater. Sci.: Mater. Med.* **2011**, *22*, 165–174.
(18) Friedlaender, G. E. *J. Bone Jt. Surg., Am. Vol.* **1987**, *69*, 786–790.
(19) Huang, Y.; Jin, X.; Zhang, X.; Sun, H.; Tu, J.; Tang, T.; Chang, J.; Dai, K. *Biomaterials* **2009**, *30*, 5041–5048.
(20) Mastrogiacomo, M.; Corsi, A.; Francioso, E.; Di Comite, M.; Monetti, F.; Scaglione, S.; Favia, A.; Crovace, A.; Bianco, P.; Cancedda, R. *Tissue Eng.* **2006**, *12*, 1261–1273.
(21) Xu, S.; Lin, K.; Wang, Z.; Chang, J.; Wang, L.; Lu, J.; Ning, C. *Biomaterials* **2008**, *29*, 2588–2596.
(22) Doostmohammadi, A.; Monshi, A.; Fathi, M. H.; Karbasi, S.; Braissant, O.; Daniels, A. U. *J. Mater. Sci.: Mater. Med.* **2011**, *22*, 2293–2300.
(23) Fathi, M. H.; Doostmohammadi, A. *J. Mater. Process. Technol.* **2009**, *209*, 1385–1391.
(24) Daculsi, G. *Biomaterials* **1998**, *19*, 1473–1478.
(25) Puleo, D. A.; Nanci, A. *Biomaterials* **1999**, *20*, 2311–2321.
(26) Bigi, A.; Fini, M.; Bracci, B.; Boanini, E.; Torricelli, P.; Giavaresi, G.; Aldini, N. N.; Facchini, A.; Sbaiz, F.; Giardino, R. *Biomaterials* **2008**, *29*, 1730–1736.
(27) Li, H.; Chen, S.; Wu, Y.; Jiang, J.; Ge, Y.; Gao, K.; Zhang, P.; Wu, L. *Int. Orthop.* **2011**, 1–7.
(28) Di Martino, A.; Liverani, L.; Rainer, A.; Salvatore, G.; Trombetta, M.; Denaro, V. *Musculoskelet. Surg.* **2011**, *95*, 69–80.
(29) Mavis, B.; Demirtas, T. T.; Gumusderelioglu, M.; Gunduz, G.; Colak, U. *Acta Biomater.* **2009**, *5*, 3098–3111.
(30) Whited, B. M.; Whitney, J. R.; Hofmann, M. C.; Xu, Y.; Rylander, M. N. *Biomaterials* **2011**, *32*, 2294–2304.
(31) Yang, L.; Hedhammar, M.; Blom, T.; Leifer, K.; Johansson, J.; Habibovic, P.; van Blitterswijk, C. A. *Biomed. Mater.* **2010**, *5*, 045002.
(32) Nandakumar, A.; Yang, L.; Habibovic, P.; van Blitterswijk, C. *Langmuir* **2009**, *26*, 7380–7387.
(33) Allo, B. A.; Rizkalla, A. S.; Mequanint, K. *Langmuir* **2010**, *26*, 18340–18348.
(34) Noh, K. T.; Lee, H. Y.; Shin, U. S.; Kim, H. W. *Mater. Lett.* **2010**, *64*, 802–805.
(35) Lu, H.; Zhang, T.; Wang, X. P.; Fang, Q. F. *J. Mater. Sci.: Mater. Med.* **2009**, *20*, 793–798.
(36) Xia, W.; Zhang, D.; Chang, J. *Nanotechnology* **2007**, *18*, 135601.
(37) Balamurugan, A.; Balossier, G.; Kannan, S.; Michel, J.; Rebelo, A. H.; Ferreira, J. M. *Acta Biomater.* **2007**, *3*, 255–262.
(38) Fathi, M. H.; Doost Mohammadi, A. *Mater. Sci. Eng., A* **2008**, *474*, 128–133.
(39) Joschek, S.; Nies, B.; Krotz, R.; Goferich, A. *Biomaterials* **2000**, *21*, 1645–1658.
(40) Rodrigues, C. V.; Serricella, P.; Linhares, A. B.; Guerdes, R. M.; Borojevic, R.; Rossi, M. A.; Duarte, M. E.; Farina, M. *Biomaterials* **2003**, *24*, 4987–4997.
(41) Karageorgiou, V.; Kaplan, D. *Biomaterials* **2005**, *26*, 5474–5491.
(42) Fratzl, P.; Gupta, H.; Paschalis, E.; Roschger, P. *J. Mater. Chem.* **2004**, *14*, 2115–2123.
(43) Yanagida, H.; Okada, M.; Masuda, M.; Ueki, M.; Narama, I.; Kitao, S.; Koyama, Y.; Furuzono, T.; Takakuda, K. *J. Biosci. Bioeng.* **2009**, *108*, 235–243.
(44) LeGeros, R. Z. *Clin. Orthop. Relat. Res.* **2002**, 81–98.
(45) Feng-Huei, L.; Chi-Chang, L.; Haw-Chang, L.; Yi-You, H.; Cheng-Yi, W.; Chung-Ming, L. *Biomaterials* **1994**, *15*, 1087–1098.
(46) Wheeler, D. L.; Montfort, M. J.; McLoughlin, S. W. *J. Biomed. Mater. Res.* **2001**, *55*, 603–612.
(47) Mistry, S.; Kundu, D.; Datta, S.; Basu, D. *Aust. Dent. J.* **2011**, *56*, 68–75.
(48) Bucholz, R.; Carlton, A.; Holmes, R. *Orthop. Clin. North Am.* **1987**, *18*, 323–334.
(49) Yamada, K.; Imamura, K.; Itoh, H.; Iwata, H.; Maruno, S. *Biomaterials* **2001**, *22*, 2207–2214.
(50) Lin, J. H. C.; Liu, M. L.; Ju, C. P. *J. Mater. Sci.: Mater. Med.* **1994**, *5*, 279–283.